ACS APPLIED MATERIALS & INTERFACES

www.acsami.org

Research Article

Huge Piezoelectric Response of LaN-based Superlattices

Minglang Hu, Chang Liu, Lee A. Burton, and Wei Ren*

Cite This: *ACS Appl. Mater. Interfaces* 2020, 12, 49805−49811

Read Online

ACCESS | Metrics & More | Article Recommendations | Supporting Information

ABSTRACT: We construct LaN-based artificial superlattices to investigate the ferroelectricity and piezoelectricity using the volume matching conditions of the parent components that soften the elastic constant C_{33} and increase the piezoelectric modulus d_{33}. The proposed superlattice consists of LaN and YN (or LaN and ScN) buckled monolayers alternately arranged along the crystallographic *c*-direction. The structure of polar wurtzite (w-LaYN/w-LaScN) is both mechanically and dynamically stable, and the computed energy barrier makes the ferroelectric polarization switching possible. We show that the epitaxial strain can modify the spontaneous ferroelectric polarization as well as d_{33}. The LaN/YN superlattice exhibits a huge piezoelectric response in the unstrained state, due to their small c/a value and extremely soft C_{33}. In addition, the epitaxial strain is revealed as effective control of the nature (indirect and direct) and value of the electronic band gap.

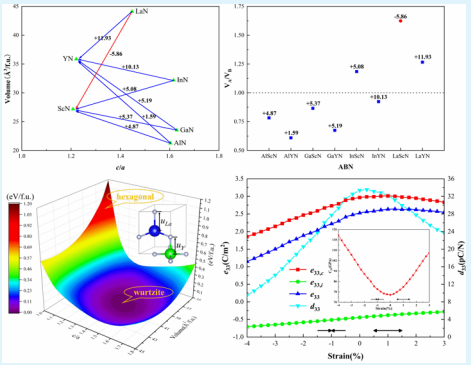

KEYWORDS: *density functional theory (DFT), ferroelectric, piezoelectric, rare earth nitrides, heterostructure*

INTRODUCTION

Piezoelectric materials can generate electric fields upon mechanical deformation and vice versa. Discovered by Pierre and Jacques Curie in tourmaline in 1880, they are widely used in modern technology. The well-known ferroelectric single crystal and polycrystalline lead zirconate titanate (PZT) based perovskites have high electromechanical coefficients and piezoelectric responses, making them suitable for micro-electromechanical system (MEMS) and nanoelectromechanical system (NEMS) devices. The power output of such devices is proportional to the piezoelectric response, but it decreases as the dielectric constant (ε) increases. However, shortcomings such as toxicity (the element lead), high cost, and high ε urge people to explore nontoxic, cheap, and high piezoelectric response materials.

Some metal nitrides have a noncentrosymmetric space group and contain the most abundant element in the atmosphere—nitrogen. The wurtzite (B4) structure w-AlN has shown great potential for application in complex sensing and mobile communication systems.[1−3] Furthermore, w-AlN has an output power equivalent to PZT and an extremely high mechanical quality factor *Q* value, making it a perfect candidate for various MEMS/NEMS devices.[4−7] However, the pure w-AlN compound still has the major disadvantage of having a low piezoelectric modulus (d_{33} = 4.11 pC/N according to our computation).

Recently, Akiyama et al.[4] discovered that the piezoelectric response of Sc-doped w-AlN was significantly enhanced. Compared with pure w-AlN, the d_{33} of $Sc_{0.5}Al_{0.5}N$ alloy increases dramatically (about 400%), which is the largest piezoelectric response of known tetrahedral semiconductors. This is due to the strong change in the strain response of the internal coordinates of atoms caused by Sc-doping, such that it increases the piezoelectric constant e_{33}. The tremendous increase in d_{33} is due to the flattening of the energy landscape caused by the competition between the parent wurtzite (w-) and hexagonal (h-) phases, which makes the elastic constant C_{33} significantly softer.[8] Tholander et al.[9] studied the piezoelectric response of w-AlN, GaN, and InN mixed with ScN or YN at a ratio of 1:1 through first-principles calculations. They explained the piezoelectric enhancement and confirmed the potential energy flattening phenomenon that caused the elastic softening of the alloys. In addition, the volume matching condition for the effective identification of new piezoelectric materials was proposed. The alloys with closely matched parent component volumes have a flatter potential energy landscape and a higher d_{33} increase. Jiang et al.[10] investigated the effect of epitaxial strain on the energetic, structural, electrical, electronic, and optical properties of a 1 × 1 AlN/ScN superlattice using ab initio calculations. The results encourage people to use dissimilar materials to make superlattices to realize the optimization and control of functionalities. Noor-A-Alam et al.[11] explored the ferroelectricity and large piezoelectric response of the AlN/ScN superlattice and found that polar w-AlScN has mechanical

Received: August 19, 2020
Accepted: October 13, 2020
Published: October 26, 2020

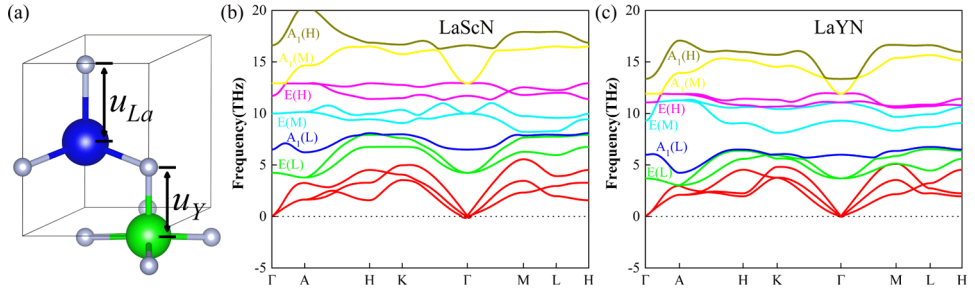

Figure 1. Schematic diagram of the structure of w-LaYN (a). The blue, green, and gray atoms are La, Y, and N, respectively. The full phonon dispersions of (b) w-LaScN and (c) w-LaYN.

and dynamic stability. Furthermore, they suggested that tensile strain is required to transform the wurtzite-derived structure into a hexagonal-derived structure so as to induce a large piezoelectric response.

We propose that even more wurtzite nitrides can be realized as excellent piezoelectric materials. For example, lanthanum (La) nitride was synthesized in a supercritical nitrogen fluid at high pressure and high temperature.[12] Ghezali et al.[13] further explored the ground state of the six structural phases of LaN using full-potential first-principles methods, including the wurtzite LaN to be discussed here. In this paper, we investigate the ground state structure of LaN and its dynamic stability, and confirm its wurtzite ground state to be isostructural to AlN, GaN, and InN, which makes it feasible to construct a LaN/YN (LaN/ScN) superlattice.[14]

COMPUTATIONAL DETAILS

We performed first-principles calculations on 1 × 1 LaN/YN, LaN/ScN, and other superlattices within the framework of density functional theory (DFT),[15,16] as implemented in the Vienna Ab initio Simulation Package (VASP)[17] using the projector augmented wave (PAW)[18,19] method. The exchange−correlation interaction was treated within the generalized gradient approximation (GGA)[20] parametrized by Perdew, Burke, and Ernzerhof (PBE).[21] The PAW potential describes the [Kr] $4d^{10}$ states of La, [Ne] states of Sc and [Ar] $3d^{10}$ states of Y as core states. A set of 6 × 6 × 4 *k*-point samplings are used for the Brillouin zone[22] in the reciprocal space by the Monkhorst−Pack scheme.[23] The cut-off energy is set to be 520 eV. In addition, all systems are relaxed completely until the Hellmann−Feynman forces on all atoms are no more than 10^{-3} eV/Å. The conjugate gradient algorithm is used to optimize the lattice parameters and internal coordinates of the structures to achieve the lowest energy configurations. By employing the residual minimization scheme, direct inversion in the iterative subspace (RMM-DIIS), the systems are geometrically optimized and the convergence for the total energy is set as 10^{-6} eV. The phonon dispersions, Born effective charges (BECs) Z_{ij}^*, piezoelectric constants e_{ij}, and elastic constants C_{ij} are calculated using density functional perturbation theory (DFPT).[24,25]

RESULTS AND DISCUSSION

By comparing the energy of the five space groups of LaN (shown in Table S1), we find that the wurtzite phase has the lowest energy, which is consistent with the work of Ghezali et al.[13] To assess its dynamic stability, we calculate the phonon dispersion of w-LaN (shown in Figure S1). There is no unstable imaginary mode in the phonon dispersion, which confirms that it is a stable ground structure. Therefore, it provides us a solid foundation to build 1 × 1 LaN/YN (LaYN) and LaN/ScN (LaScN) superlattices.

As shown in Figure 1a, the presently investigated LaYN (LaScN) superlattice has hexagonal parent compounds LaN and YN (ScN). The primitive lattice vectors of the direct Bravais lattice are

$$\mathbf{a}_1 = a\left(\frac{1}{2}\mathbf{x} - \frac{\sqrt{3}}{2}\mathbf{y}\right)$$

$$\mathbf{a}_2 = a\left(\frac{1}{2}\mathbf{x} + \frac{\sqrt{3}}{2}\mathbf{y}\right)$$

$$\mathbf{a}_3 = c\mathbf{z}$$

Among them, *a* (in-plane) and *c* (out-of-plane) are two lattice parameters. *c*/*a* is defined as the axial ratio. **x**, **y**, and **z** are the unit vectors along the Cartesian axes. The primitive unit cell contains four atoms, namely, Y (Sc) and La located at $\mathbf{r}_1$ and $\mathbf{r}_2$ and two N atoms located at $\mathbf{r}_3$ and $\mathbf{r}_4$, with

$$\mathbf{r}_1 = 0$$

$$\mathbf{r}_2 = \frac{2}{3}\mathbf{a}_1 + \frac{1}{3}\mathbf{a}_2 + \frac{1}{2}\mathbf{a}_3$$

$$\mathbf{r}_3 = u_{\mathrm{Y(Sc)}}\mathbf{a}_3$$

$$\mathbf{r}_4 = \frac{2}{3}\mathbf{a}_1 + \frac{1}{3}\mathbf{a}_2 + \left(\frac{1}{2} + u_{\mathrm{La}}\right)\mathbf{a}_3$$

The LaYN (LaScN) superlattice consists of LaN and YN (ScN) buckled monolayers, alternately arranged along the crystallographic *c*-direction. The quantities $u_{\mathrm{Y(Sc)}}$ and u_{La} are the dimensionless internal parameters, where $u_{\mathrm{Y(Sc)}}$ is connecting the Y(Sc) and N atoms that are nearest neighbors along the *z*-axis, and the u_{La} is binding La ions and the N atoms along $\mathbf{a}_3$.

Table S2 shows the parameters of LaN, YN, LaYN, and LaScN superlattices. Since w-LaYN and w-LaScN are new structures, their mechanical stability are checked according to the standard of the hexagonal crystal structure:[26] $C_{11} > C_{12}$, $2C_{13}^2 < C_{33}(C_{11} + C_{12})$, $C_{44} > 0$, $C_{66} > 0$. Additionally, in the light of the elastic constants provided in Table S3, it can be seen that w-LaYN and w-LaScN are mechanically stable. The phonon dispersions of w-LaYN and w-LaScN are also calculated as shown in Figure 1b,c. There is no unstable imaginary mode in the phonon dispersions, which confirms that w-LaYN and w-LaScN are stable structures or structurally metastable. From the group theory analysis, there are nine optical modes at Γ with irreducible representation: $\Gamma_{\mathrm{opt}} = 3E +$

https://dx.doi.org/10.1021/acsami.0c14969
ACS Appl. Mater. Interfaces 2020, 12, 49805−49811

$3A_1$, where E modes are doubly degenerate. The L, M, and H in Figure 1b,c are used for labeling the low, medium, and high frequencies for both E and A_1 modes. The A_1 modes represent the atomic vibration along the *c*-direction, while the atoms vibrate in-plane for the E modes. Three A_1 modes along the Γ−A direction in the first Brillouin zone are shown in Figure S2a.

Note that the wurtzite structure has a 6mm point group in the international notation, $c/a = \sqrt{8/3}$ and $u = 0.375$ in the ideal form. The c/a ratios of w-LaYN and w-LaScN are both lower than the ideal value, leading to spontaneous polarization in the [0001] direction. Our calculated spontaneous polarization along the *c*-direction P_3 for w-LaYN (w-LaScN) is 0.73 C/m^2 (1.07 C/m^2), with an energy barrier of 0.15 eV (0.53 eV). The studied superlattices both have spontaneous polarization larger than $BaTiO_3$ (~0.25 C/m^2) and even comparable with $PbTiO_3$ (~0.88 C/m^2).[27] Therefore, w-LaYN should be a promising candidate for ferroelectricity, while the energy barrier of w-LaScN might be somewhat high for practical ferroelectric devices. (More calculational details of ferroelectric polarization can be found in the Supporting Information.)

As is well known, ferroelectric materials should be able to generate piezoelectric responses but not vice versa. We find that the e_{33} values of LaN-based superlattices are larger than that of w-LaN. A similar situation occurs in other ternary alloys as well,[9] and our superlattices here are alloys with a specific composition and configuration. We calculate the properties of w-AlN, GaN, InN, and their superlattices to confirm their conclusion (shown in Table 1). The C_{33} and e_{33} results of group-III nitrides are essentially in good agreement with literature data.[9,28] The e_{33} value of the AlYN superlattice is lower than that of the parent nitride and the C_{33} value of the LaScN superlattice is higher than that of the parent nitride. In contrast, the other superlattices have higher e_{33} and lower C_{33} than their parent nitride, resulting in an enhancement in piezoelectric modulus d_{33}. This proves the volume matching condition to establish enhanced piezoelectricity. It is worth noting that the volumes of the parent nitrides of AlYN and LaScN superlattices are extremes (i.e., maximal YN + minimal AlN or minimal ScN + maximal LaN), where the d_{33} value of LaScN is reduced, as shown in Figure 2. Furthermore, we can find that as V_A/V_B approaches 1, the d_{33} value increases. While AlYN superlattice's $V_A/V_B = 0.61$, it only increases the d_{33} value by 1.59 pC/N; LaScN superlattice's $V_A/V_B = 1.62$ even decreases the d_{33} value by 5.86 pC/N. We recommend that a parent nitride with a larger d_{33} value should be used to establish the superlattice. Although the Δd_{33}(%) values of GaScN, GaYN, and InYN superlattices are relatively large, the superlattice d_{33} is still small overall due to the small d_{33} value of the parent nitride. Yet, the LaYN superlattice does not have this disadvantage since LaN already possesses a large d_{33} value and incorporating YN could further increase it by 56%.

Table 1. Piezoelectric Constant e_{33}, Elastic Constant C_{33}, and Piezoelectric Modulus d_{33} for Parent Binaries and 1 × 1 Superlattices with ScN and YN

material	e_{33} (C/m^2)	e_{33}/e_{33}^{parent}	C_{33} (GPa)	C_{33}/C_{33}^{parent}	d_{33} (pC/N)	Δd_{33} (%)
AlN	1.46		354.89		4.11	
GaN	0.44		358.58		1.22	
InN	0.87		205.73		4.21	
LaN	1.78		82.98		21.45	
AlScN	1.78	1.22	198.02	0.56	8.98	4.87 (118%)
AlYN	1.20	0.82	211.21	0.60	5.70	1.59 (39%)
GaScN	1.33	3.02	201.95	0.56	6.59	5.37 (440%)
GaYN	1.12	2.55	175.24	0.49	6.41	5.19 (425%)
InScN	1.52	1.75	163.36	0.79	9.29	5.08 (121%)
InYN	1.72	1.98	119.61	0.58	14.34	10.13 (241%)
LaScN	1.81	1.02	116.31	1.40	15.59	−5.86 (−27%)
LaYN	2.53	1.42	75.70	0.91	33.38	11.93 (56%)

To understand the piezoelectric behavior from a microscopic perspective, e_{33} is usually decomposed into "clamped ion" and "internal strain" contributions[29,30]

$$e_{33} = e_{33,c} + e_{33,i}$$

The clamped-ion $e_{33,c}$ is evaluated without allowing additional relaxation of the relative atomic coordinates that would be induced by the strain. In contrast, the internal strain $e_{33,i}$ only measures the contribution of these internal deformations to the piezoelectric response. We find that $e_{33,i}$ increases with increasing lattice parameters from the compressive to tensile strains. On the other hand, $e_{33,c}$ is positively related to the epitaxial strain of −4−1% (1.75%) and negatively related to the tensile epitaxial strain of 1% (1.75%) to 3% for the LaYN (LaScN) superlattice in Figure 3a,b. We also show the relation trend of e_{33} and c/a values in Figure S3 to explain this increase under the epitaxial strain of −4−1.5% (1%). Momida et al.[31] discovered the effect of lattice parameters on piezoelectric constants in wurtzite materials. According to the energy potential energy landscapes in Figure 3c,d, we can find that when the c/a value becomes lower than about 1.35 (1.42), the small-volume LaYN (LaScN) superlattice tends to have the hexagonal structure, which also leads to a decrease in e_{33}. Although for LaYN, e_{33} increases from zero epitaxial to 1.25% tensile strain, we find that C_{33} is minimum at zero strain, which is different from the cases of other superlattices. The c/a = 1.403 of the LaYN superlattice without strain is small, making the energy landscape more flattened by the competition between the parent wurtzite and hexagonal phases. Moreover, e_{33} increases at 0−1.75% epitaxial strain and C_{33} is minimum at 1.5% epitaxial strain for the LaScN superlattice.

The d_{33} of the hexagonal structure is defined as[32]

$$d_{33} = \frac{e_{33} - \frac{2C_{31}}{C_{11}C_{12}}e_{31}}{C_{33} - \frac{2C_{31}^2}{C_{11}C_{12}}}$$

in which the in-plane parameters e_{31}, C_{11}, C_{12}, and C_{31} can be fixed so that d_{33} is approximately equal to e_{33}/C_{33}. w-LaYN has a huge d_{33} (33.38 pC/N) under no strain, although the epitaxial tensile strain does not increase the d_{33} value, while it effectively reduces the spontaneous ferroelectric polarization. Therefore, w-LaYN is an ideal piezoelectric material in the normal state under no applied strain. The maximum d_{33} (19.27 pC/N) is at 1.75% epitaxial strain for the LaScN superlattice.

Interestingly, the epitaxial strain also acts as effective control for the nature (indirect and direct) and value of the electronic band gap as shown in Figure 4. Under all strains, the contribution of the conduction band minimum (CBM) comes from the *s* orbitals of all atoms, while the contribution of the valence band maximum (VBM) varies with strain, leading to a change in the trend of the band gap value and nature. Under

https://dx.doi.org/10.1021/acsami.0c14969
ACS Appl. Mater. Interfaces 2020, 12, 49805−49811

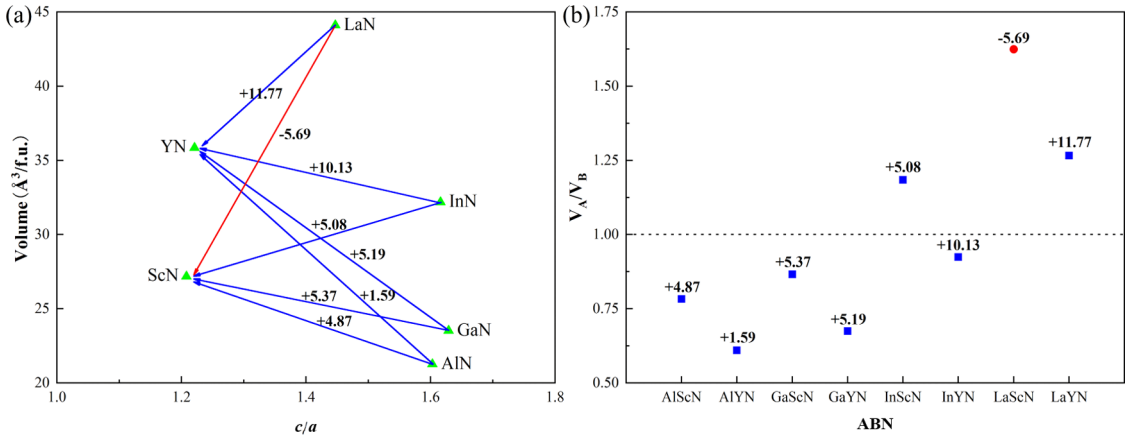

Figure 2. (a) Volume and c/a ratio of the superlattices considered in this paper. (b) Volume ratio of AN to BN (V_A/V_B) (A is Al, Ga, In, La, and B is Sc, Y). The values around the blue lines (data points) show the superlattices with increased Δd_{33} and the value around the red line (data point) shows that with decreased Δd_{33}.

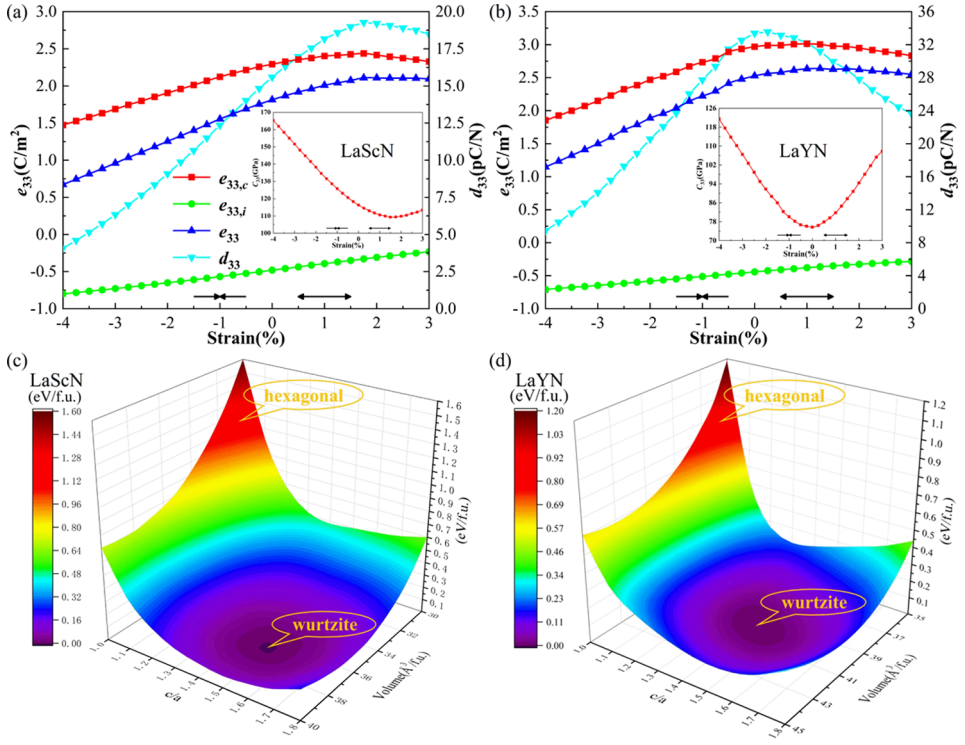

Figure 3. Clamped-ion contribution $e_{33,c}$, internal strain component $e_{33,i}$, piezoelectric constant e_{33}, and piezoelectric modulus d_{33} as a function of epitaxial strain for the epitaxial strain ranging between −4 and 3% in (a) w-LaScN and (b) w-LaYN. The inset shows the variation of the elastic constant C_{33}. The potential energy landscape of (c) LaScN and (d) LaYN superlattices versus c/a and volume with both wurtzite and hexagonal phases being indicated.

3% epitaxial strain, the VBM is mainly contributed by the p_z orbital of N_{La} (the N connected with La along the z-axis), which is similar to the paraelectric phase structure when we analyzed the electronic origin of ferroelectricity. Under large epitaxial tensile strain, the superlattice changes from the ferroelectric phase to the paraelectric phase, which causes the p_z orbital of N_{La} to hybridize with the d_{z^2} of La. Under small tensile strain or compressive strain, the VBM is contributed by other N p_x or p_y orbitals. For the LaYN superlattice under an epitaxial tensile strain of 2−3%, the direct band gap could be present at the Γ point.

It is worth mentioning that, in realistic experiments, an appropriate epitaxial strain may be induced by growing nitrides on another nitride substrate or adjusted by doping the nitride substrate.[33−36] Recently, high-quality artificial nitride samples with designed epitaxial strain have been achieved.[37−41] In addition, there may also be suitable parent components in metal oxides to construct superlattices, such as ZnO and MgO. In fact, piezoelectric ZnO/MgO films have been prepared in experiments, and related measurements have been reported.[42−47]

CONCLUSIONS

In summary, from the ground state wurtzite structure of LaN, we have constructed wurtzite-like 1 × 1 LaN-based artificial superlattices that are both mechanically and dynamically stable

https://dx.doi.org/10.1021/acsami.0c14969
ACS Appl. Mater. Interfaces 2020, 12, 49805−49811

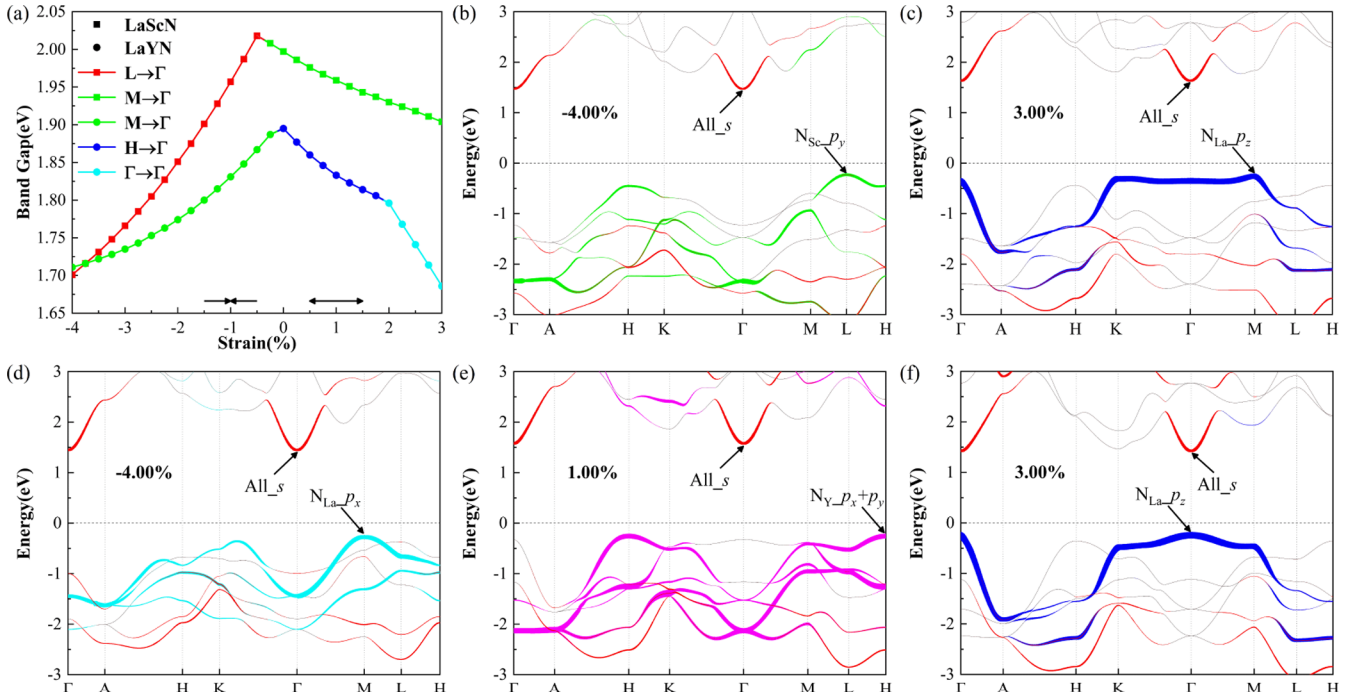

Figure 4. (a) Nature (indirect and direct) and value of the electronic band gap of LaN-based superlattices as a function of epitaxial strain for the epitaxial strain ranging between −4 and 3%. The projected energy band structures of the LaScN superlattice change with the epitaxial strain values of (b) −4.00% and (c) 3.00%. The LaYN superlattice changes with the epitaxial strain values of (d) −4.00%, (e) 1.00%, and (f) 3.00%.

and show spontaneous ferroelectric polarization. The volume matching condition of the parent components allows the softening of the elastic constant C_{33} and increases the piezoelectric modulus d_{33}, resulting in a huge d_{33} value of w-LaYN. In addition, epitaxial tensile strain is found to introduce a significant change in the spontaneous ferroelectric polarization and d_{33} as well. The strain is also demonstrated to effectively control the nature (indirect and direct) and value of the electronic band gap. Our results provide guidance for designing nitride superlattice ferroelectric and piezoelectric materials.

■ ASSOCIATED CONTENT

Supporting Information

The Supporting Information is available free of charge at https://pubs.acs.org/doi/10.1021/acsami.0c14969.

Energy comparison of different structures of LaN (Table S1); related structural parameters and physical properties discussed in the article (Tables S2 and S3); dynamic stability prediction of LaN from phonon spectra (Figure S1); vibration mode of A_1 and phonon dispersion with considering the nonanalytic correction term (Figure S2); e_{33} versus lattice constant ratio (c/a) of the LaN-based superlattices (Figure S3); ferroelectric energy barrier and polarization value of the LaN-based superlattices (Figure S4); phonon and electronic origin of ferroelectricity (Figures S5 and S6) (PDF)

■ AUTHOR INFORMATION

Corresponding Author

Wei Ren − *Physics Department, Shanghai Key Laboratory of High Temperature Superconductors, State Key Laboratory of Advanced Special Steel, International Centre of Quantum and Molecular Structures, Shanghai University, Shanghai 200444, China;* orcid.org/0000-0001-7317-3867; Email: renwei@shu.edu.cn

Authors

Minglang Hu − *Physics Department, Shanghai Key Laboratory of High Temperature Superconductors, State Key Laboratory of Advanced Special Steel, International Centre of Quantum and Molecular Structures, Shanghai University, Shanghai 200444, China;* orcid.org/0000-0003-1662-2915

Chang Liu − *Physics Department, Shanghai Key Laboratory of High Temperature Superconductors, State Key Laboratory of Advanced Special Steel, International Centre of Quantum and Molecular Structures, Shanghai University, Shanghai 200444, China*

Lee A. Burton − *Physics Department, Shanghai Key Laboratory of High Temperature Superconductors, State Key Laboratory of Advanced Special Steel, International Centre of Quantum and Molecular Structures, Shanghai University, Shanghai 200444, China;* orcid.org/0000-0002-0647-5483

Complete contact information is available at: https://pubs.acs.org/10.1021/acsami.0c14969

Notes

The authors declare no competing financial interest.

■ ACKNOWLEDGMENTS

This work was supported by the National Natural Science Foundation of China (Grant nos. 51861145315, 51672171, 51911530124, and 12074241), the Shanghai Municipal Science and Technology Commission Program (Grant no. 19010500500), the Austrian Research Promotion Agency (FFG, Grant no. 870024, project acronym MagnifiSens), and the Independent Research Project of State Key Laboratory of Advanced Special Steel and Shanghai Key Laboratory of Advanced Ferrometallurgy at Shanghai University.

REFERENCES

(1) Rinaldi, M.; Zuniga, C.; Zuo, C.; Piazza, G. Super-high-frequency Two-port AlN Contour-mode Resonators for RF Applications. *IEEE TTrans. Ultrason., Ferroelect., Freq. Contr.* **2010**, *57*, 38−45.

(2) Muralt, P.; Antifakos, J.; Cantoni, M.; Lanz, R.; Martin, F. Is There a Better Material for Thin Film BAW Applications than AlN? *IEEE Ultrason. Symp.* **2005**, *1*, 315−320.

(3) Loebl, H.; Klee, M.; Metzmacher, C.; Brand, W.; Milsom, R.; Lok, P. Piezoelectric Thin AlN Films for Bulk Acoustic Wave (BAW) Resonators. *Mater. Chem. Phys.* **2003**, *79*, 143−146.

(4) Akiyama, M.; Kamohara, T.; Kano, K.; Teshigahara, A.; Takeuchi, Y.; Kawahara, N. Enhancement of Piezoelectric Response in Scandium Aluminum Nitride Alloy Thin Films Prepared by Dual Reactive Cosputtering. *Adv. Mater.* **2009**, *21*, 593−596.

(5) Sinha, N.; Wabiszewski, G. E.; Mahameed, R.; Felmetsger, V. V.; Tanner, S. M.; Carpick, R. W.; Piazza, G. Piezoelectric Aluminum Nitride Nanoelectromechanical Actuators. *Appl. Phys. Lett.* **2009**, *95*, No. 053106.

(6) Xiong, C.; Sun, X.; Fong, K. Y.; Tang, H. X. Integrated High Frequency Aluminum Nitride Optomechanical Resonators. *Appl. Phys. Lett.* **2012**, *100*, No. 171111.

(7) Piazza, G.; Felmetsger, V.; Muralt, P.; Olsson, R. H., III; Ruby, R. Piezoelectric Aluminum Nitride Thin Films for Microelectromechanical Systems. *MRS Bull.* **2012**, *37*, 1051−1061.

(8) Tasnádi, F.; Alling, B.; Höglund, C.; Wingqvist, G.; Birch, J.; Hultman, L.; Abrikosov, I. A. Origin of the Anomalous Piezoelectric Response in Wurtzite $Sc_xAl_{1-x}N$ Alloys. *Phys. Rev. Lett.* **2010**, *104*, No. 137601.

(9) Tholander, C.; Abrikosov, I. A.; Hultman, L.; Tasnádi, F. Volume Matching Condition to Establish the Enhanced Piezoelectricity in Ternary $(Sc,Y)_{0.5}(Al,Ga,In)_{0.5}N$ Alloys. *Phys. Rev. B: Condens. Matter Mater. Phys.* **2013**, *87*, No. 094107.

(10) Jiang, Z.; Paillard, C.; Vanderbilt, D.; Xiang, H.; Bellaiche, L. Designing Multifunctionality via Assembling Dissimilar Materials: Epitaxial AlN/ScN Superlattices. *Phys. Rev. Lett.* **2019**, *123*, No. 096801.

(11) Noor-A-Alam, M.; Olszewski, O. Z.; Nolan, M. Ferroelectricity and Large Piezoelectric Response of AlN/ScN Superlattice. *ACS Appl. Mater. Interfaces* **2019**, *11*, 20482−20490.

(12) Hasegawa, M.; Niwa, K.; Yagi, T. Synthesis of New La Nitrides at High Pressure and Temperature. *Solid State Commun.* **2007**, *141*, 267−272.

(13) Ghezali, M.; Amrani, B.; Cherchab, Y.; Sekkal, N. Structural and Electronic Properties of LaN. *Mater. Chem. Phys.* **2008**, *112*, 774−778.

(14) Ghezali, M.; Sekkal, N. Structural, Electronic, and Optical Properties of $(LaN)_n/(ScN)_n$ and $(LaN)_n/(YN)_n$ Superlattices. *Chin. J. Phys.* **2013**, *51*, 1098−1106.

(15) Tong, B.; Sham, L. Application of A Self-consistent Scheme Including Exchange and Correlation Effects to Atoms. *Phys. Rev.* **1966**, *144*, No. 1.

(16) Hohenberg, P.; Kohn, W. Inhomogeneous Electron Gas. *Phys. Rev.* **1964**, *136*, No. B864.

(17) Kresse, G.; Hafner, J. Ab Initio Molecular Dynamics for Liquid Metals. *Phys. Rev. B: Condens. Matter Mater. Phys.* **1993**, *47*, 558−561.

(18) Blöchl, P. E. Projector Augmented-wave Method. *Phys. Rev. B: Condens. Matter Mater. Phys.* **1994**, *50*, 17953−17979.

(19) Kresse, G.; Joubert, D. From Ultrasoft Pseudopotentials to the Projector Augmented-Wave Method. *Phys. Rev. B: Condens. Matter Mater. Phys.* **1999**, *59*, 1758−1775.

(20) Burke, K.; Perdew, J. P.; Ernzerhof, M. Why the Generalized Gradient Approximation Works and How to Go beyond It. *Int. J. Quantum Chem.* **1997**, *61*, 287−293.

(21) Hammer, B.; Hansen, L. B.; Nørskov, J. K. Improved Adsorption Energetics within Density-functional Theory Using Revised Perdew-Burke-Ernzerhof Functionals. *Phys. Rev. B: Condens. Matter Mater. Phys.* **1999**, *59*, No. 7413.

(22) Blöchl, P. E.; Jepsen, O.; Andersen, O. K. Improved Tetrahedron Method for Brillouin-zone Integrations. *Phys. Rev. B: Condens. Matter Mater. Phys.* **1994**, *49*, No. 16223.

(23) Monkhorst, H. J.; Pack, J. D. Special Points for Brillouin-zone Integrations. *Phys. Rev. B: Condens. Matter Mater. Phys.* **1976**, *13*, 5188−5192.

(24) Baroni, S.; Resta, R. Ab Initio Calculation of the Macroscopic Dielectric Constant in Silicon. *Phys. Rev. B: Condens. Matter Mater. Phys.* **1986**, *33*, 7017−7021.

(25) Gajdoš, M.; Hummer, K.; Kresse, G.; Furthmüller, J.; Bechstedt, F. Linear Optical Properties in the Projector-augmented Wave Methodology. *Phys. Rev. B: Condens. Matter Mater. Phys.* **2006**, *73*, No. 045112.

(26) Mouhat, F.; Coudert, F.-X. Necessary and Sufficient Elastic Stability Conditions in Various Crystal Systems. *Phys. Rev. B: Condens. Matter Mater. Phys.* **2014**, *90*, No. 224104.

(27) Ederer, C.; Spaldin, N. A. Effect of Epitaxial Strain on the Spontaneous Polarization of Thin Film Ferroelectrics. *Phys. Rev. Lett.* **2005**, *95*, No. 257601.

(28) Bernardini, F.; Fiorentini, V.; Vanderbilt, D. Spontaneous Polarization and Piezoelectric Constants of III-V Nitrides. *Phys. Rev. B: Condens. Matter Mater. Phys.* **1997**, *56*, No. R10024.

(29) Bellaiche, L.; Vanderbilt, D. Intrinsic Piezoelectric Response in Perovskite Alloys: PMN-PT versus PZT. *Phys. Rev. Lett.* **1999**, *83*, No. 1347.

(30) Bellaiche, L. Piezoelectricity of Ferroelectric Perovskites from First Principles. *Curr. Opin. Solid State Mater. Sci.* **2002**, *6*, 19−25.

(31) Momida, H.; Oguchi, T. Effects of Lattice Parameters on Piezoelectric Constants in Wurtzite Materials: A Theoretical Study Using First-principles and Statistical-Learning Methods. *Appl. Phys. Express* **2018**, *11*, No. 041201.

(32) Tholander, C.; Tasnadi, F.; Abrikosov, I. A.; Hultman, L.; Birch, J.; Alling, B. Large Piezoelectric Response of Quarternary Wurtzite Nitride Alloys and Its Physical Origin from First Principles. *Phys. Rev. B: Condens. Matter Mater. Phys.* **2015**, *92*, No. 174119.

(33) Tamariz, S.; Martin, D.; Grandjean, N. AlN Grown on Si (1 1 1) by Ammonia-molecular Beam Epitaxy in the 900−1200 °C Temperature Range. *J. Cryst. Growth* **2017**, *476*, 58−63.

(34) Rao, M.; Kim, D.; Mahajan, S. Compositional Dependence of Phase Separation in InGaN Layers. *Appl. Phys. Lett.* **2004**, *85*, 1961−1963.

(35) Le Louarn, A.; Vézian, S.; Semond, F.; Massies, J. AlN Buffer Layer Growth for GaN Epitaxy on (1 1 1) Si: Al or N First? *J. Cryst. Growth* **2009**, *311*, 3278−3284.

(36) Yang, M.; Wang, W.; Lin, Y.; Yang, W.; Li, G. Epitaxial Growth of High Quality AlN Films on Si Substrates. *Mater. Lett.* **2016**, *182*, 277−280.

(37) Wu, X.; Elsass, C.; Abare, A.; Mack, M.; Keller, S.; Petroff, P.; DenBaars, S.; Speck, J.; Rosner, S. Structural Origin of V-defects and Correlation with Localized Excitonic Centers in InGaN/GaN Multiple Quantum Wells. *Appl. Phys. Lett.* **1998**, *72*, 692−694.

(38) Cho, H.; Lee, J.; Yang, G.; Kim, C. Formation Mechanism of V Defects in the InGaN/GaN Multiple Quantum Wells Grown on GaN Layers with Low Threading Dislocation Density. *Appl. Phys. Lett.* **2001**, *79*, 215−217.

(39) Lekhal, K.; Damilano, B.; Ngo, H.; Rosales, D.; De Mierry, P.; Hussain, S.; Vennéguès, P.; Gil, B. Strain-compensated (Ga,In)N/(Al,Ga)N/GaN Multiple Quantum Wells for Improved Yellow/Amber Light Emission. *Appl. Phys. Lett.* **2015**, *106*, No. 142101.

(40) Koleske, D.; Fischer, A.; Bryant, B.; Kotula, P.; Wierer, J. On the Increased Efficiency in InGaN-based Multiple Quantum Wells Emitting at 530−590 nm with AlGaN Interlayers. *J. Cryst. Growth* **2015**, *415*, 57−64.

(41) Al Muyeed, S. A.; Sun, W.; Wei, X.; Song, R.; Koleske, D. D.; Tansu, N.; Wierer, J. J., Jr Strain Compensation in InGaN-based Multiple Quantum Wells Using AlGaN Interlayers. *AIP Adv.* **2017**, *7*, No. 105312.

https://dx.doi.org/10.1021/acsami.0c14969
ACS Appl. Mater. Interfaces 2020, 12, 49805−49811

(42) Bhattacharya, P.; Das, R. R.; Katiyar, R. S. Fabrication of Stable Wide-band-gap ZnO/MgO Multilayer Thin Films. *Appl. Phys. Lett.* **2003**, *83*, 2010−2012.
(43) Emanetoglu, N. W.; Muthukumar, S. N.; Pan, W.; Wittstruck, R. H.; Yimin, C.; Yicheng, L. $Mg_xZn_{1-x}O$: A New Piezoelectric Material. *IEEE TTrans. Ultrason., Ferroelect., Freq. Contr.* **2003**, *50*, 537−543.
(44) Yu, H. K.; Baik, J. M.; Lee, J.-L. Self-Connected and Habitually Tilted Piezoelectric Nanorod Array. *ACS Nano* **2011**, *5*, 8828−8833.
(45) Martínez-Gutiérrez, D.; Velasco, V. R. Transverse Acoustic Waves in Piezoelectric ZnO/MgO and GaN/AlN Fibonacci-periodic Superlattices. *Surf. Sci.* **2014**, *624*, 58−69.
(46) Lee, H.-J.; Kang, J.-W.; Hong, S.-H.; Song, S.-H.; Park, S.-J. $Mg_xZn_{1-x}O$/Ag/$Mg_xZn_{1-x}O$ Multilayers as High-Performance Transparent Conductive Electrodes. *ACS Appl. Mater. Interfaces* **2016**, *8*, 1565−1570.
(47) Park, S.-H.; Hong, W.-P.; Kim, J.-J. Piezoelectric and Spontaneous Polarization Effects on Exciton Binding Energy and Light Emission Properties of Wurtzite ZnO/MgO Quantum Dots. *Solid State Commun.* **2017**, *261*, 21−25.

https://dx.doi.org/10.1021/acsami.0c14969
ACS Appl. Mater. Interfaces 2020, 12, 49805−49811